Biomedical Physics & Engineering Express

ENDORSED BY IPEM Institute of Physics and Engineering in Medicine

PAPER • OPEN ACCESS

Characterization of time-varying magnetic fields and temperature of helium gas exit during a quench of a human magnetic resonance system

Biomedical Physics & Engineering Express

OPEN ACCESS

RECEIVED
21 February 2019

REVISED
15 May 2019

ACCEPTED FOR PUBLICATION
20 May 2019

PUBLISHED
24 June 2019

PAPER

Characterization of time-varying magnetic fields and temperature of helium gas exit during a quench of a human magnetic resonance system

Nicola Pace[1], Leonardo Ricci[1,2], Mario Scotoni[2], Alessio Perinelli[2] and Jorge Jovicich[1]

[1] CIMeC, University of Trento, Rovereto, Italy
[2] Department of Physics, University of Trento, Trento, Italy

E-mail: nicola.pace@unitn.it

Keywords: magnetic resonance Imaging, quench, safety

Abstract

The quench of a human magnetic resonance imaging system is a critical event that may occur spontaneously, as an accident or purposely in response to an emergency. Although a magnet's quench presents its own risks, little experimental data is available in this respect. In this study, the programmed quench of a human MRI scanner was used to measure the induced time varying magnetic fields (dB/dt) inside the bore in order to evaluate cardiac stimulation risks during a quench. Additionally, we measured the exit temperature of the helium gas, to evaluate potential implications in quench pipe design. The maximum dB/dt was 360 mT s^{-1} at the center of the magnet, far below the cardiac stimulation threshold (20 T s^{-1}). The helium exit temperature reached 35 K, perhaps implying further considerations about quench pipe designs. Replication of similar experiments on programmed quenches, specially in high-field MRI systems, will be useful to further characterize quench risks.

1. Introduction

Magnetic Resonance Imaging (MRI) is a well-established imaging technology used for both clinical diagnostics and research to characterize tissue properties non-invasively. Its medical use around the world is steadily increasing: between 2010 and 2015 the number of MRI exams per year increased from 45 to 59 per 1000 inhabitants in the Economic Co-operation and Development (OECD) countries, an increase of 30% (OECD 2019a). In the same period, the number of MRI scanners per 1million inhabitants went from about 12 to almost 15 (OECD 2019b).

The widespread use of MRI in clinical practice makes safety considerations particularly important. Nowadays, most clinical MRI scanners installed around the world are based on the superconducting principle: liquid helium at 4.2 K is used as a cryogenic to keep the coil of the static magnetic field (B_0) superconductive. The sudden loss of the coil superconductivity is called a quench, during which the rise of the coil's temperature induces the fast evaporation of the liquid helium and results in the fast decay of B_0. The expansion ratio of helium is such that 1 l of liquid helium is transformed in 757 l of helium gas (Wilks 1967). Therefore, since standard clinical scanners can store between 1500 and 2000 liters of liquid helium, MRI systems are designed with a quench pipe system that can safely release the high-pressure low temperature cryogenics outside the building (Medicines and Healthcare Products Regulatory Agency 2015, Department of Veterans Affairs 2008).

The quench of a clinical MRI system, activated either manually during an emergency or spontaneously due to an accident or a system failure, may present health risks to a patient inside the magnet. One quench risk relates to the strong temporal derivative of the static field that a patient might experience if lying inside the scanner during a quench (B_0 decays into the level of Earth's magnetic field). Fast magnetic field variations may induce peripheral nerve stimulation and cardiac stimulation. During a standard MRI acquisition, such stimulation risks are associated to the fluctuations of the magnetic field gradients used for spatial encoding. It has been shown that magnetic field gradients can indeed stimulate peripheral nerves, and that by beyond a perception threshold, they can induce discomfort, pain and even cardiac stimulation (Reilly 1989, Egerter 1990, Kanal *et al* 1990, Ham

et al 1997). The International Electrotechnical Commission (IEC), in its International Standard for the basic safety and essential performance of magnetic resonance equipment (IEC 2015), introduced three different MRI magnetic gradient working levels: normal mode, in which some patients may experience Peripheral Nerve Stimulation (PNS) but uncomfortable PNS is prevented; Controlled mode, in which some patients may experience uncomfortable PNS; Experimental mode, in which exposure is restricted to prevent cardiac stimulation. According to the same IEC Standard, the PNS gradient threshold can be calculated empirically as $20 \cdot \left(1 + \frac{0.36}{t}\right)$ T s^{-1}, where t is the length of the stimulation. On the other hand, in order to prevent cardiac stimulation, the threshold $\frac{20}{(1 - e^{-t/3})}$ T s^{-1} should be respected. It is easy to calculate that while for short pulses (i.e. below several 100 ms) the threshold of cardiac stimulation is one order of magnitude higher than PNS threshold, for long pulses such difference vanishes, and one can assume that any stimulation exceeding 20 T s^{-1} has the potential to cause cardiac stimulation, with possible severe harm to the person experiencing the magnetic field gradient. While during normal MRI activity the magnetic gradient field fluctuations are applied only for some fractions of ms, during a quench the stimulation might stand for a longer time. For this reason, the characterization of the magnetic field decay dynamics is important to evaluate the potential risk of cardiac stimulation of a patient lying inside an MRI scanner during a quench. Regulatory bodies have different approaches to address the cardiac stimulation risk during aquench, sometimes deeming it as negligible (Medicines and Healthcare Products Regulatory Agency 2015), sometimes raising concerns of possible cardiac stimulation (Istituto Nazionale per l'Assicurazione contro gli Infortuni sul Lavoro (INAIL), 2015) without citing any experimental results as support. There are studies in the literature that have characterized various aspects of a quench in superconducting magnets (for example, (Bottura 2013, Bottura and Zienkiewicz 1992)). However, to the best of our knowledge, there is no experimental evidence in literature that helps to clarify the magnitude of the cardiac stimulation risk during a quench of a human MRI scanner.

Another quench risk relates to the possibility of helium gas leakage from the quench pipe. This risk is related to the pipe system failing to withstand both the pressure and the temperature of the helium gas. While mechanical risks due to pressure are known and well tackled by the previously mentioned regulatory bodies, risks due to temperature are not explicitly mentioned, and to our knowledge there are no studies in the literature that characterize, during a quench, the helium gas temperature at the quench pipe exit of a human MRI system.

As part of the decommissioning of a human 4T MRI system (Bruker Medspec 4T), we exploited the opportunity of a planned quench to measure the following parameters during the event: i) the variation of the magnetic field inside the bore; ii) the temperature of the gas exhausted by the quench pipe. The experimental setups built to conduct these measurements are here described in details for possible use in future MRI quench induced opportunities.

2. Measurement setup

One of the two goals of this work was to measure the decay of the magnetic field inside an MRI scanner bore. Many different magnetic sensing techniques are employed both in laboratories and in technological applications (Ripka 2001). The choice of a specific sensor depends on the required bandwidth, the range of field intensities to measure, and the desired resolution. Hall sensors are the most common kind of devices, widely used in commercial applications (Popovic 2004) due to their low cost and ease of integration inside electronic chips. Hall sensors are well suited to measure medium and high fields (Ripka 2001, Ripka and Janosek 2010) starting from fractions of mT. For fields in the μT range, anisotropic magnetoresistive sensors can achieve resolutions down to 10 nT with tens of kHz of bandwidth (Bertoldi *et al* 2005). Very small magnetic fields require more demanding technologies such as SQUIDs. For the measurement discussed in this work, the sensors had to operate and measure in the presence of a field of few T. Moreover, the key quantity that we are interested in is the time derivative of the field, rather than its absolute value. For these reasons, an affordable solution was to build macroscopic (~0.1 m) induction sensors, each consisting of a coil pair. The four coils, two for each sensor and each one connected to an independent ADC, exploit Faraday's law to directly sample the induced electromotive force during the quench. The two sensors were positioned close to and within the MRI bore. To have an independent additional measure of the magnetic field decay that could be compared with the coil measures, we positioned a commercial magnetometer aside the scanner bore. The setup to measure the time evolution of the main 'static' magnetic field during the quench is thoroughly described in appendix A.1.

As shown in figure 1, the first coil pair (A–B) was placed at the bore entrance, where a static magnetic field of 0.3 T was measured, while the other pair (C–D) was placed at the center of the bore, namely where the magnetic field is most uniform. The magnetometer (F. W. Bell, Model 8010 Gauss/Teslameter) relies on a temperature–compensated Hall probe placed within the shielded room where the MRI scanner is hosted. The exact position of the probe is displayed in figure 1. Its orientation was adjusted to maximize the measured magnetic field, which amounted to 26.39(5) mT before the quenching procedure. The magnetometer sampled the magnetic field at a rate of 5 Hz and stored the measurements in an internal logger. The position

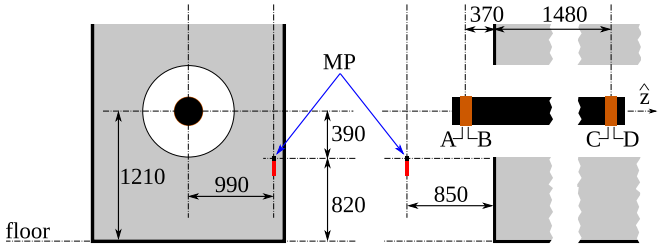

Figure 1. Schematic frontal and lateral cross-sectional views of the magnet indicating the relative position of the magnetometer probe (MP, black square on top of a red rod) and of the two coil pairs A–B, C–D relatively to the MRI scanner bore (600 mm). Dimensions are given in mm.

of the magnetometer probe was determined by the closest location that it could have with respect to the magnet bore while allowing to safely position the console needed to read the probe inside the magnet room.

The second main goal of this study was to measure the temperature of the cryogenics at the exit of the quench pipe. The measurement was carried out by using two Pt100 resistors. The two sensors, labeled with P and Q in figure 2, were placed at a distance of 0.10 m and 1.10 m from the output of the Helium pipe, respectively. The details of the temperature measurement setup are described in appendix A.2.

3. Results

3.1. Magnetic field measurements

The measurements of the induced dB_z/dt signal during the quench in the the four coils are shown in figure 3 and figure 4. Figure 5 shows the field directly measured by the Hall probe outside the bore. The rescaled numeric time derivative of this last quantity is shown in figure 6 together with the time derivative directly measured by the outermost coil (red curve of figure 3). In all plots, the time $t = 0$ corresponds to the start of the quenching process.

The results from figures 3 and 5 show that the extinction of the magnetic field occurs in about 40 s after the quench is initiated. The maximum absolute value of the field derivative occurred at different times for the outer coils (A and B, red and green curves of figure 3) compared with the two coils at the center of the bore (figure 4). This delay is most likely due to the spatially inhomogeneous extinction of the current within the superconducting coils. The maximum absolute value of dB_z/dt was measured by coil C (blue curve of figure 4) and amounted to 0.36 T s^{-1} approximately 18 s after the quench. As far as the coils outside the bore are concerned, the maximum measured field derivative was 22 mT/s approximately 12 s after the quench.

3.2. Temperature measurements

The temperature measured by the two sensors is shown in figure 7. As for the magnetic field, time is measured in seconds after the triggering of the quenching procedure. In figure 8, three pictures, taken by means of the thermal camera (FLIR T650sc) during the Helium outflow, are displayed. Both in the region of the Helium cloud and the pipe, the false–color scale is saturated at its lowest detectable temperature (−40° C), consistently with the quantitative assessment of temperature reported in the plot of figure 7. After approximately 100 s from the quench start, the temperature 0.10 m outside the quench pipe reached values as low as 35(2) K, and remained below 50 K for almost 2 minutes. The temperature drop was less marked at 1.10 m, where values as low as 150 K were reached though a more noisy trend. Environmental temperature was recovered about 3 minutes after the quench.

4. Discussion

4.1. Magnetic field measurements

While during normal MRI activity the magnetic gradient field fluctuations are applied only for some fractions of ms, our work shows how during a quench the stimulation can stand for several 100 ms. Nonetheless, in this study we found that the maximum magnetic field gradient experienced inside the magnet bore during the quench is 0.35 T s^{-1}, while at the bore entrance the maximum gradient slightly exceeds 0.02 T s^{-1}. Such values are significantly lower (~60 and ~1000 times, respectively) than the threshold introduced by IEC even considering a pulse of infinite duration (20 T s^{-1}). It seems unlikely that other human MRI scanners (with static fields equal or smaller than 4 T), characterized by different manufacturing solutions, may have a B_0 decay that is fast enough to exceed the cardiac stimulation threshold. Nonetheless, it would be desirable that magnet manufacturers provide a formal declaration in which the maximum levels of dB/dt possibly experienced by a person inside the magnet during a quench are stated, in order to rule out any possible health emergency arising from such issue.

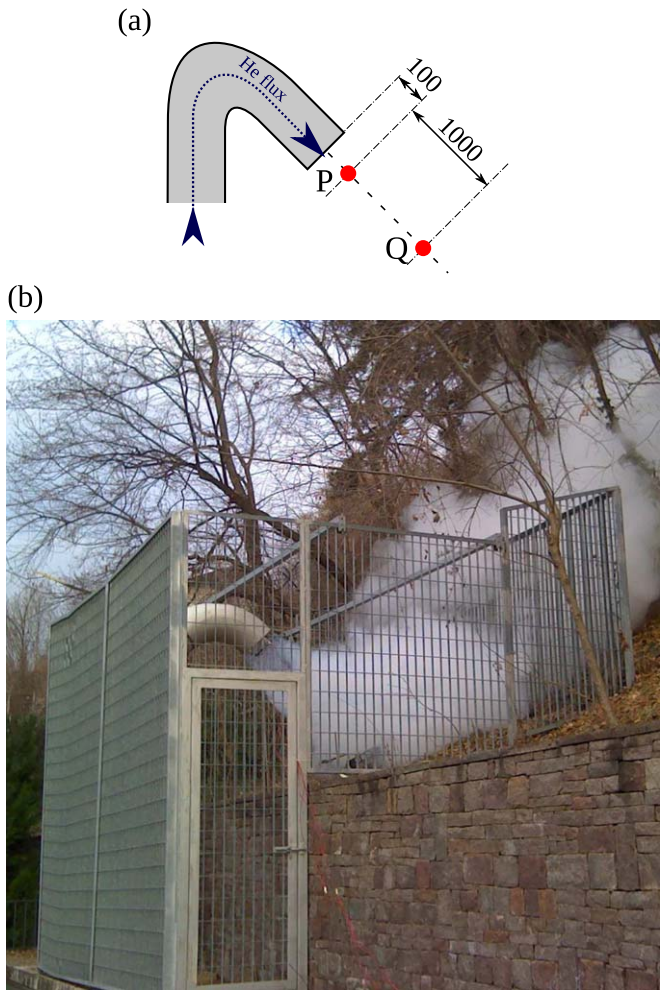

Figure 2. (a) Schematic view of the quench exhaust pipe indicating the relative positions (in mm) of the two temperature sensors P and Q. (b) View of the Helium outflow pipe during the quench, caged within a safety area.

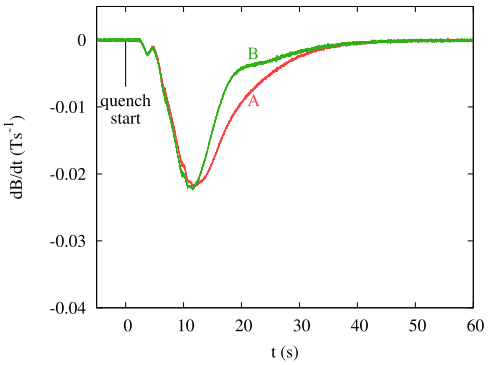

Figure 3. dB_z/dt measured by the coils at the bore's entrance: the red curve corresponds to the outermost coil (labelled with A in figure A1); the green curve corresponds to the second coil (B) outside the bore. Time $t = 0$ corresponds to the start of the quenching process.

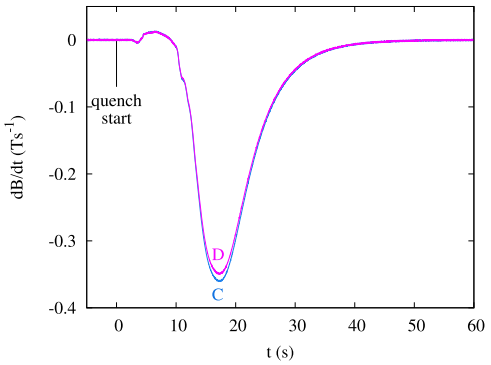

Figure 4. dB_z/dt measured by the coils at the magnet's center: the blue and magenta curves correspond to the two coils C and D at the center of the bore, respectively. Time $t = 0$ corresponds to the start of the quenching process. It is worth noticing that the y–axis covers a 10 times larger range of values compared to figure 3.

4.2. Temperature measurements

The quench pipe terminal is known to be a place in which severe risk of frostbite and asphyxia occurs, due to the huge amount of Helium gas produced by the quench and canalized outside of the building by the quench pipe. For such reason, the pipe usually ends in locations not reachable by any unauthorized person, and its visual inspection is often suggested by manufacturers and regulatory bodies at least once a year. In addition, care is due in the building of the entire length of the pipe, in order to ensure that no leakage will

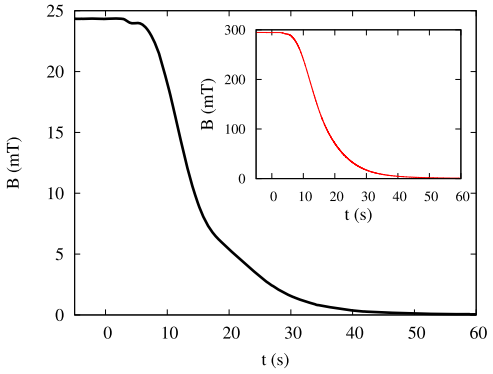

Figure 5. Magnetic field decay during the quench measured by the magnetometer outside the bore (black line). Time $t = 0$ corresponds to the start of the quenching process. Inset: magnetic field resulting by the numerical integration of the dB_z/dt signal measured by coil A (red line).

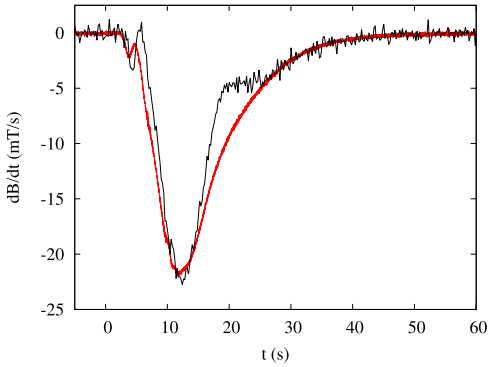

Figure 6. Time derivative of the field directly measured by the outermost coil (red curve) and numerically–computed from the field measured by the magnetometer (black curve; see figure 5) and rescaled by a factor 50. This factor is due to the larger distance of the magnetometer to the magnet as compared to the outermost coil.

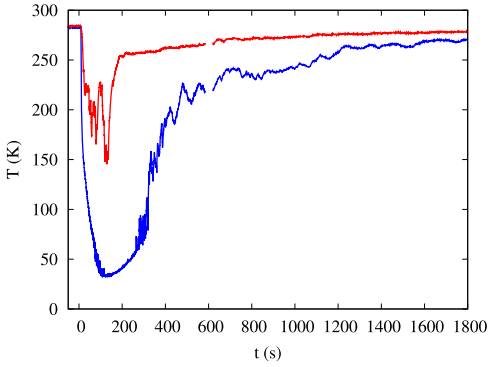

Figure 7. Temperature measured by the two sensors (see figure 2). The blue curve corresponds to the sensor placed close to the pipe output (0.1 m), while the red curve corresponds to the sensor placed 1.1 meter away from the output.

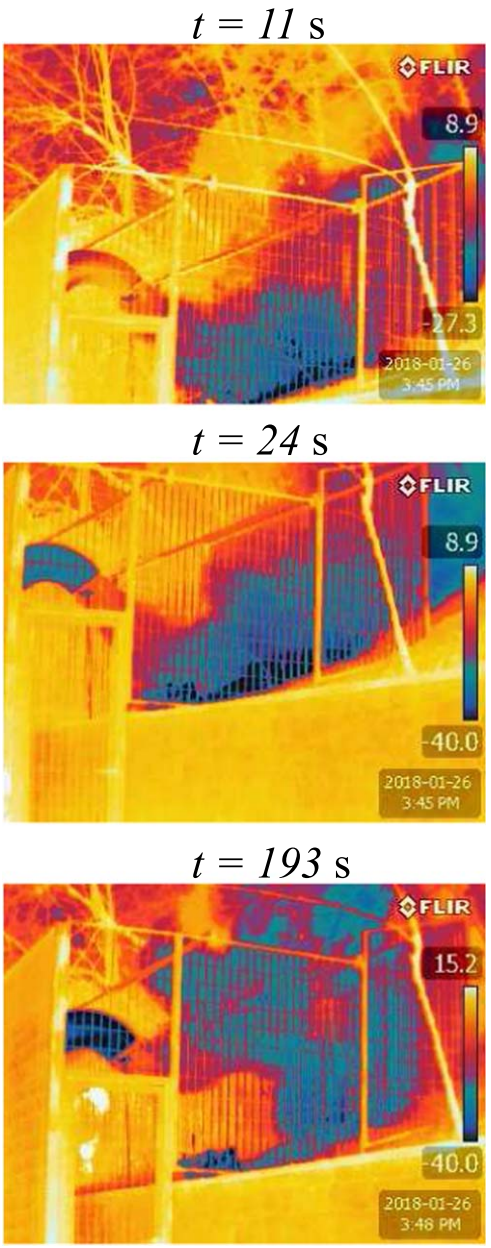

Figure 8. False–color images, taken by means of the thermal camera, of the Helium outflow pipe, at different times after the start of the quenching procedure.

occur with subsequent uncontrolled dispersion of Helium gas. Quench pipes are usually manufactured and installed under the guidance of the magnet manufacturer, which indicates section diameters, length, curves, and type of assembly to be used. To prevent damages caused by the supposedly high pressure reached during the quench inside the quench pipe, particular attention is given to the materials and the fitting solutions. Typically, Aluminum or stainless steel are used, and different parts of the pipe are connected by means of weld joints or flanges and gaskets to avoid gas leakage. Our results suggest that, in addition to gas pressure, also exhaust gas temperature can represent a cause of damage during a quench event. As an example, in the case of a quench pipe assembled by means of flanges, the installed insulation gaskets are often made by Polytetrafluoroethylene (PTFE). PTFE is an extremely versatile polymeric

material, characterized by a wide working temperature range, as it maintains high strength, toughness and self-lubrication at low temperatures down to 5 K. Despite this, PTFE loses its flexibility at temperatures below 194 K (Rae and Dattelbaum 2004, Dupont 1996), and many of the PTFE products seem not to be certified for a usage below 33.2K (for example (Chemours (n.d.))), a temperature close to the one that we measured in our study for helium gas at the quench pipe exit during a quench of a human MRI system. Due to thermal stress of metal parts as a consequence of the sudden temperature decrease and the decreased elasticity of PTFE, the behaviour of PTFE gaskets during a quench might therefore become unpredictable. Therefore, it would be desirable that quench pipe manufacturers include in their certifications information about the suitability of the materials used to withstand low temperatures. Finally, the results collected through the sensor positioned 1.10 m from the pipe terminal show that spikes of very low temperature are reached also at such distance, confirming and highlighting the importance of restricting the area around the quench pipe terminal.

4.3. Study limitations

The dB/dt values that can be measured through the method described in the present work are expected to be dependent on parameters such as the magnet structure and the magnitude of the static magnetic field. However, the small values of dB/dt measured on a 4 T magnet suggest that such variations should not pose a threat to the conclusions outlined below. Replications of similar measurements on other MRI systems would be of interest to further validate our conclusions and test the magnetic field decay model presented here. With regards of the measurements carried out at the exit of the quench pipe, it can be argued that the Helium gas temperature depends on the characteristics of the pipe (total length, curves, diameter) and the total amount of Helium stored within the magnet at the moment of the quench. While our results cannot be directly generalized to other quench pipes, they do represent a standard case (e.g. the quench pipe is certified to be safe by the manufacturer). Also in this case, the replication of the performed measurements on other systems is of clear interest.

5. Conclusions

According to IEC, the thresholds for peripheral nerve and cardiac stimulation after some 100 ms asymptotically tends to 20 T s^{-1}. The dB_z/dt values measured in this study (0.35 T s^{-1} inside the magnet bore, 0.02 T s^{-1} at the bore entrance) are more than one order of magnitude lower than this threshold, suggesting that cardiac stimulation does not make up a concern during the quench of a human MRI system like the one used. Given the dynamics of an induced quench and the magnitude of the difference between our results and the cardiac stimulation threshold, it is unlikely that other human MRI scanners (with static fields equal or smaller than 4 T), though characterized by different manufacturing solutions, can go through a collapse of B_0 fast enough to entail gradient values of the order of those needed to trigger cardiac stimulation. Nonetheless, further experiments are needed on other human MRI systems to confirm these findings. Our measurements of the Helium temperature at the exit of the quench pipe showed that can be as low as low as 35 K. Awareness of these low temperatures is important for the design and installation specification of quench pipes.

Appendix A. Materials and methods

This appendix describes the two experimental setups used in the induced quench of a 4T MRI system (Bruker Medspec 4T): a) a system to measure the time derivative of the main static field inside the bore of the magnet; b) a system to measure the temperature of the cryogenic gases at the exit of the quench pipe.

A.1. Setup for the measurement of the time evolution of the main 'static' magnetic field during the quench

The magnetic field within the MRI scanner bore has a cylindrical symmetry. The symmetry axis is henceforth referred to as the z–axis. In order to measure the time derivative of the field component parallel to the z–axis, a setup consisting of two pairs of coaxial coils was assembled. A diagram of the coil setup is shown in figure A1. The coils were wound around a 110 mm diameter cylindrical plastic pipe, and were made by an insulated copper wire of 0.315 mm diameter. The axis of the coils setup coincided (within ~10 mm) with the axis of the MRI scanner bore. Each coil consisted of 105 windings, so that the equivalent area is 1.004(5) m^2. Consequently, a time derivative of 1 T s^{-1} of the z–component of the magnetic field is expected, according to Faraday's law, to generate 1 V of electromotive force on the coil. As mentioned above, the first coil pair (A–B) was placed at the bore entrance, while the other pair (C–D) was placed at the center of the bore, namely where the magnetic field is most uniform (see figure A1). The reason for using a coil pair instead of a single coil in each location was to allow measurement redundancy given the uniqueness of the event investigated. The availability of a two–fold sensor, and thus the minimization of the probability of getting no data in case of a single, malfunctioning sensor, largely overcomes undesired cross–talk effects between the coils belonging to the same pair, as explained below.

Each coil had a measured self–inductance $L = 1.54(1)$ mH and a measured resistance of 8.2 Ω. The mutual inductance between the two coils

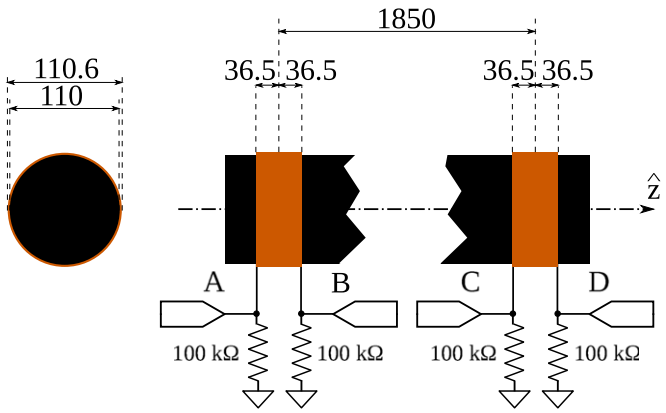

Figure A1. Diagram of the plastic pipe (black) and the four coils (in red) used to measure the induced dB_z/dt signal during the quench at two positions inside the magnet bore. The coils A and B were positioned close to the magnet bore exit, and the coils C and D were positioned approximately at the center of the magnet. Dimensions are reported in mm.

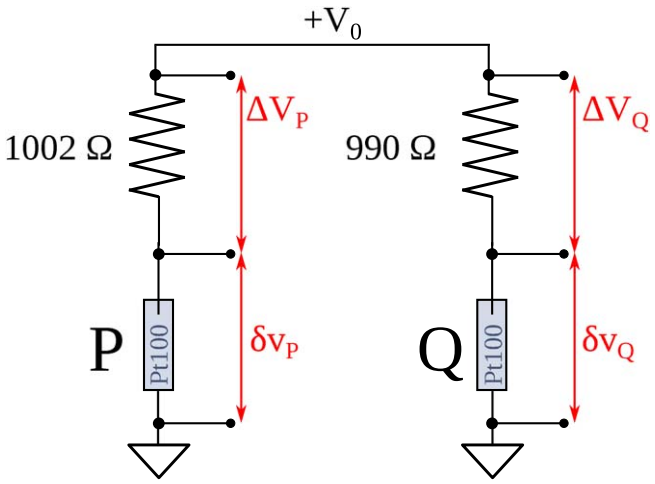

Figure A2. Diagram of the resistance readout circuit. The measured voltage drops are highlighted.

belonging to the same pair was measured to be $M = 0.60(1)$ mH. The induced electromotive force across each coil was measured by connecting it to an input of an acquisition board (National Instrument, USB–6003). The sampling was carried out by a 16–bit ADC at a rate of 12.5 kHz. A resistor $R = 100$ kΩ was connected in parallel to each coil in correspondence of the board input. The characteristic time scale of the inductive effect was $L/R \approx M/R \approx 10^{-8}$ s. Because the field variations were expected to occur over a time scale of 0.1 s, inductive effects were completely negligible.

Because the characteristic frequency of the inductor–resistor system is of order $\sim$ 100 MHz, the bandwidth of the measured dB_z/dt signal is limited by the acquisition board's sampling frequency. The input range of the ADC was $\pm$10 V; its declared accuracy and system noise were 6 mV and 0.4 mV rms, respectively. The dB_z/dt signal produced by each of the four coils was low–pass filtered and resampled by computing the average of successive, non–overlapping segments of 125 samples. The resulting bandwidth was therefore 100 Hz.

In order to synchronize the magnetometer with the computer–based acquisition system, before and after the quenching procedure a suitable magnetic signal was delivered at exactly the same time to one of the coil pairs and to the magnetometer. This operation was carried out by feeding two small solenoids connected in series with a short train of square–wave current pulses ($\sim$1 Hz). Each pulse produced a square–wave signal on the magnetometer and a voltage spike in the coils.

A.2. Setup for the measurement of the temperature close to the Helium outflow pipe

Each temperature sensor was connected in series with a $\sim$1 kΩ resistor, placed $\sim$ 10 m away from the pipe and supplied with a constant voltage $V_0 = 10.056(1)$ V. The circuit diagram is displayed in figure A2. The voltage drop across each resistor, labeled with δv_P, ΔV_P, δv_Q, ΔV_Q in figure A2, were sampled with a second

acquisition board (National Instrument USB–6003). The sampling rate was 5 Hz up to 580 s after the start of the quenching, and 1 Hz from 620 s on. The resistance of the P and Q sensors was straightforwardly computed as $R_P = 1002\,\Omega \cdot \delta v_P/\Delta V_P$ and $R_Q = 990\,\Omega \cdot \delta v_Q/\Delta V_Q$, respectively. Finally, the resistance values of the Pt100 sensors as a function of time were converted to temperature values by means of a suitable calibration.

ORCID iDs

Nicola Pace https://orcid.org/0000-0001-5370-0674

References

Bertoldi A, Bassi D, Ricci L, Covi D and Varas S 2005 Magnetoresistive magnetometer with improved bandwidth and response characteristics *Review of Scientific Instruments* **76** 065106

Bottura L 2013 Magnet quench 101 *CERN Yellow Report CERN-2013-006* 1–9

Bottura L and Zienkiewicz O C 1992 Quench analysis of large superconducting magnets. II: model validation and application *Cryogenics* **32** 719–28

Chemours (n.d.). Ptfe products datasheets. Accessed 2019-04-19. URL: https://www.chemours.com/Teflon_Industrial/en_US/tech_info/prodinfo_ptfe.html

Department of Veterans Affairs 2008 VA design guide: magnetic resonance imaging (MRI) Accessed 2018-11-23. URL: https://www.wbdg.org/FFC/VA/VADEGUID/mri.pdf

Dupont 1996 Teflon PTFE fluoropolymer resin: properties handbook

Egerter D E 1990 MR nerve stimulation: new safety concern? *Diagnostic Imaging* **12** 127–31 PMID: 10149364

Ham C L G, Engels J M L, van de Wiel G T and Machielsen A 1997 Peripheral nerve stimulation during MRI: effects of high gradient amplitudes and switching rates *Journal of Magnetic Resonance Imaging* **7** 933–7

IEC 2015 IEC 60601-2-33:2010+AMD1:2013+AMD2:2015 CSV: medical electrical equipment—part 2–33: particular requirements for the basic safety and essential performance of magnetic resonance equipment for medical diagnosis

Istituto Nazionale per l'Assicurazione contro gli Infortuni sul Lavoro (INAIL) 2015 Indicazioni operative dell'Inail per la gestione della sicurezza e della qualità in Risonanza Magnetica Page 64. Accessed 2019-02-05. URL: https://www.inail.it/cs/internet/docs/allegato_indicazioni_operative_risonanza.pdf

Kanal E, Shellock F G and Talagala L 1990 Safety considerations in MR imaging *Radiology* **176** 593–606

Medicines and Healthcare Products Regulatory Agency 2015 Safety guidelines for magnetic resonance imaging equipment in clinical use Accessed 2018-11-23. URL: https://assets.publishing.service.gov.uk/government/uploads/system/uploads/attachment_data/file/476931/MRI_guidance_2015_-_4-02d1.pdf

OECD 2019a Magnetic resonance imaging (MRI) exams (indicator) Accessed 2019-02-05. URL: https://www.oecd-ilibrary.org/content/data/1d89353f-en (https://doi.org/10.1787/1a72e7d1-en)

OECD 2019b Magnetic resonance imaging (MRI) units Accessed 2019-02-05. URL: https://www.oecd-ilibrary.org/content/data/1a72e7d1-en (https://doi.org/10.1787/1a72e7d1-en)

Popovic R S (ed) 2004 *Hall Effect Devices* 2nd edn (Bristol and Philadelphia: Institute of Physics)

Rae P J and Dattelbaum D M 2004 The properties of poly (tetrafluoroethylene) (PTFE) in compression *Polymer* **45** 7615–25

Reilly J P 1989 Peripheral nerve stimulation by induced electric currents: exposure to time-varying magnetic fields *Medical and Biological Engineering and Computing* **27** 101–10

Ripka P (ed) 2001 *Magnetic Sensors and Magnetometers* (Norwood, United States: Artech House Publishers)

Ripka P and Janosek M 2010 Advances in magnetic field sensors *IEEE Sensors Journal* **10** 1108–16

Wilks J 1967 *The Properties of Liquid and Solid Helium* (Oxford: Clarendon)